Available online at www.sciencedirect.com
ScienceDirect
Combustion and Flame 153 (2008) 525–539
Combustion and Flame
www.elsevier.com/locate/combustflame

A numerical study of the stability of one-dimensional laminar premixed flames in inert porous media

M.A.A. Mendes, J.M.C. Pereira, J.C.F. Pereira *

Technical University of Lisbon/Instituto Superior Técnico, Mechanical Engineering Department, LASEF, Av. Rovisco Pais 1, 1049-001 Lisbon, Portugal

Received 13 June 2007; received in revised form 28 January 2008; accepted 11 March 2008

Available online 22 April 2008

Abstract

This work presents a numerical study of the stabilization diagram of methane/air premixed flames in a finite porous media foam with a uniform ambient temperature. A set of steady computations are considered, using a 1D numerical model that takes into account solid and gas energy equations as well as chemistry and radiation models. The present results show that both stable and unstable solutions, for upper and lower flames, exist either at the surface or submerged in the porous matrix. The influence of the 1D computational domain, boundary conditions, and gas/solid interface treatment on the stability of the calculated flames is also discussed. A linearized version of the discrete-ordinates radiation model is included in the linear stability analysis to discuss the influence of radiation on the stability of the flames. The full stabilization diagram and the linear stability analysis provide information on the stability of the flames, pointing to the existence of unstable upstream surface flames as well as unstable submerged flames on the downstream part of the porous media.

Keywords: Premixed combustion; Inert porous media; Linear stability analysis; Radiation; Flame stabilization

1. Introduction

Premixed combustion in inert porous media combines a number of positive features, such as high burning rates, wide dynamic power range, large flame stability limits, and reduced NO_x and CO emissions compared to free flames [1–3]. The solid matrix enhances heat recirculation due to the transport of energy by radiation and conduction, which are orders of magnitude higher than in free flames. Since the pioneer studies, see, e.g., Weinberg [4], the outlined excess enthalpy combustion has suggested the use of highly conductive porous materials to exchange heat between products and reactants, see [5,6], and several numerical calculations, see, e.g., [7–10], have highlighted the relevance of the radiative energy transport mechanism in the porous media combustion.

The mechanism of premixed flame stabilization within porous media constitutes a complex and relevant phenomenon for the operation and safety of burners and combustors. Buckmaster and Takeno [11] studied the blowoff and flashback problem by applying activation energy asymptotics analysis to a simplified porous media combustion model. They verified the possibility of two distinct combustion modes, corresponding to submerged and surface flames, and they suggested that in order for flame stability to exist, the flame speed must increase for flames displaced

* Corresponding author.
E-mail address: jcfpereira@ist.utl.pt (J.C.F. Pereira).

0010-2180/$ – see front matter
doi:10.1016/j.combustflame.2008.03.010

Nomenclature

A	Arrhenius pre-exponential factor
a_s	volumetric surface area
C_p	specific heat capacity
D	diffusion coefficient
E	activation energy
H_s	surface heat transfer coefficient
H_v	volumetric heat transfer coefficient
h	specific enthalpy
I	radiation intensity
L	length
MW	molecular weight
Q_r	radiative flux
R	universal gas constant
S_L	flame speed
s	direction vector
T	temperature
t	time
u	velocity
x	position
Y	mass fraction

Greek symbols

β	extinction coefficient
δ	species perturbation amplitude
ε	solid emissivity
θ	eigenvalue
λ	thermal conductivity
μ	direction angle cosine
ρ	density
σ	Stefan–Boltzmann constant
τ	optical depth, temperature perturbation amplitude
Φ	phase function
ϕ	solid porosity
ω	scattering albedo
$\dot{\omega}$	chemical production rate

Superscripts

$'$	perturbing quantity
–	mean quantity

Subscripts

0	solid inlet
b	black body
cr	critical
f	flame
fuel	fuel species (CH_4)
g	gas mixture
i	direction index
k	species index
L	solid outlet
o	free flame
ox	oxidizer species (O_2)
s	porous solid

downstream. The extinction, flashback, and blowoff limits of surface flames were studied by Hanamura and Echigo [7]. By performing transient calculations for a porous media combustion flame, they presented flame stabilization diagrams for submerged and surface flames and showed that for some values of equivalence ratio there is a flashback window in the velocity for surface flames.

Experimental investigation related to the stabilization diagrams of premixed flames in porous foams is very scarce. To the authors' knowledge, just a few experimental studies have been conducted. Among them, Min and Shin [12] experienced the existence of two types of stable submerged flames, with different flame speeds and temperatures, at the same location in the upstream part of a honeycomb ceramic burner. They concluded that the low-burning-velocity and low-temperature flames are different from the excess enthalpy flames. A stabilization diagram, obtained with a 1D model, predicted both types of flames in the downstream part of the burner, but these were not observed in the experiments, presumably due to heat loss. Lee et al. [13] also used a 1D numerical model to investigate both types of flames. The flames with higher burning velocity and temperature were named upper flames and the others were named lower flames. They performed experiments similar to those of [12], but using another burner configuration. Stable submerged lower flames at the downstream location were only possible to find with circumferential external heating. These experiments showed the existence of unstable submerged flames in the downstream region of the burner if no external heating was supplied. Kotani et al. [14] investigated the stability and combustion characteristics of a combustor system for extended flow ranges, based on excess enthalpy flames. Two ceramic filters were placed upstream and downstream of the porous media combustion zone to reduce the radiative heat losses, and their studies revealed the existence of three distinct flames stabilized inside, ahead of, and behind the porous solid. The flame stability was found to depend on the heat recirculation, as well as on the heat losses of the burner system.

More recently, Diamantis et al. [15] investigated submerged and surface flame stabilization within porous media, and their computational results suggested that submerged upper flames are unstable in

the downstream region of a porous burner, in agreement with [11]. Lammers and de Goey [16] used 1D stationary and transient calculations to study flashback on surface porous burners, and stabilization diagrams were obtained for submerged and surface flames similar to those presented by [7]. They have shown that there is a flashback window in the velocity if the radiation temperature of the environment becomes too high. During the unsteady flashback process, they found that flames, apparently stable, can exist in areas where the burning velocity increases while the flame is displaced upstream. According to the argument presented by [11], the burning velocity should decrease in order for stable flames to exist; however, the simplified model used in [11] may not describe the heat transfer process in real porous media combustion accurately.

Linear stability analysis is a commonly used tool to study the development of instabilities in premixed combustion systems. The two intrinsic instability mechanisms associated with premixed flame propagation are hydrodynamic instability and diffusive–thermal instability [17]. Normally, theoretical studies about burner-stabilized premixed flames just consider the diffusive–thermal instabilities to analyze the effect of heat losses on the flame [18,19]. The same will be done in this study, because it is believed that the influence of the porous solid on the flames is of thermal nature. The diffusive–thermal effects can originate pulsating or cellular instabilities, but due to the one-dimensional character of the linear stability analysis performed in this study, the cellular structures are suppressed. If 3D structures were allowed, the stability behavior could change; however, in the study of Kurdyumov and Matalon [18] about surface flames stabilized in a porous-plug burner, the flame instabilities were found to correspond to planar pulsations.

From the previous studies, it can be noted that the flame stabilization problem in porous media is not a clarified issue, and some unanswered questions can still be asked. First, several assumptions can be used to model the interface between the porous solid and gaseous surroundings, and their influence on the flame location and stability requires to be analyzed. Second, the solid radiation is an important phenomenon in porous media combustion, which cannot be neglected, and its influence on the flame stabilization mechanism deserves to be investigated. Finally, to the authors' knowledge, a linear stability study of combustion in porous media accounting for radiation has not yet been conducted. These three topics constitute the main objectives of this work.

This paper is organized as follows. A 1D model is presented to simulate combustion within porous media and a linear stability analysis is performed. A linearized version of the discrete-ordinates radiation model was included in the linear stability analysis to discuss the stability of submerged and surface steady flames. In addition, the influence of the various treatments for the interface solid/gas at inlet and outlet porous planes and radiation models on the stability of the calculated flames is discussed.

2. Theoretical modelling

2.1. Governing equations

We consider premixed laminar combustion of a stoichiometric methane/air mixture in a SiC ceramic foam of length L, see Fig. 1. We also assume a one-dimensional geometry, inert homogeneous porous material, constant pressure, and negligible catalytic effects. With these assumptions the governing equations for mass, species, and energy (of the gas and solid phases) are

Continuity equation

$$\frac{\partial(\phi\rho_{\mathrm{g}})}{\partial t}+\frac{\partial(\phi\rho_{\mathrm{g}}u)}{\partial x}=0. \tag{1}$$

Species transport equation

$$\phi\rho_{\mathrm{g}}\frac{\partial Y_k}{\partial t}+\phi\rho_{\mathrm{g}}u\frac{\partial Y_k}{\partial x}-\frac{\partial}{\partial x}\left(\phi\rho_{\mathrm{g}}D_k\frac{\partial Y_k}{\partial x}\right)-\phi\dot{\omega}_k\mathrm{MW}_k=0. \tag{2}$$

Gas energy equation

$$\phi\rho_{\mathrm{g}}C_{\mathrm{pg}}\frac{\partial T_{\mathrm{g}}}{\partial t}+\phi\rho_{\mathrm{g}}uC_{\mathrm{pg}}\frac{\partial T_{\mathrm{g}}}{\partial x}-\frac{\partial}{\partial x}\left(\phi\lambda_{\mathrm{g}}\frac{\partial T_{\mathrm{g}}}{\partial x}\right)-\phi\sum_k\rho_{\mathrm{g}}C_{\mathrm{pk}}D_k\frac{\partial Y_k}{\partial x}\frac{\partial T_{\mathrm{g}}}{\partial x}+\phi\sum_k\dot{\omega}_k h_k\mathrm{MW}_k+H_{\mathrm{v}}(T_{\mathrm{g}}-T_{\mathrm{s}})=0. \tag{3}$$

Solid energy equation

$$\frac{\partial((1-\phi)\rho_{\mathrm{s}}C_{\mathrm{ps}}T_{\mathrm{s}})}{\partial t}-\frac{\partial}{\partial x}\left((1-\phi)\lambda_{\mathrm{s}}\frac{\partial T_{\mathrm{s}}}{\partial x}\right)-H_{\mathrm{v}}(T_{\mathrm{g}}-T_{\mathrm{s}})+\frac{\partial Q_{\mathrm{r}}}{\partial x}=0. \tag{4}$$

The porosity ϕ represents the volume fraction of the gas phase; therefore in regions outside the porous media ϕ equals 1, and otherwise ϕ equals the solid porosity ϕ_{s}.

The gas and solid equations, (3) and (4), are connected by the convection heat transfer term $H_{\mathrm{v}}(T_{\mathrm{g}}-T_{\mathrm{s}})$, representing the heat exchange between the two phases. An irreversible one-step chemical reaction ($CH_4+2O_2\rightarrow CO_2+2H_2O$) was assumed and the species production rates $\dot{\omega}_k$ are given in the Arrhenius form by the equation

$$\dot{\omega}_k=-\alpha_k\frac{\rho_{\mathrm{g}}^2}{\mathrm{MW}_{\mathrm{fuel}}}AY_{\mathrm{fuel}}Y_{\mathrm{ox}}e^{-E/(RT_{\mathrm{g}})}, \tag{5}$$

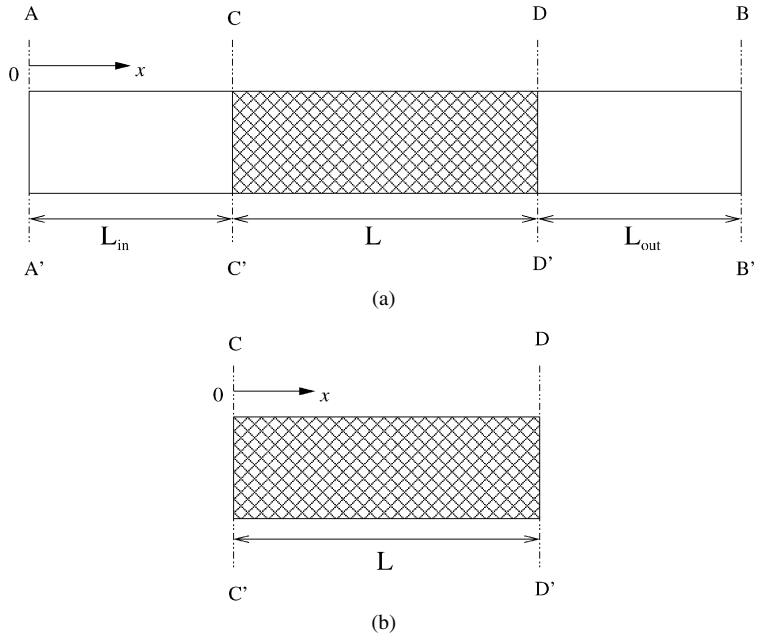

Fig. 1. Computational domains ($L = 1.0$ cm; $L_{in} = L_{out} = 2.0$ cm). (a) Gas–solid–gas (GSG) domain, with inlet/outlet boundaries at AA′ and BB′, respectively; (b) solid (S) domain, with inlet/outlet boundaries at CC′ and DD′, respectively.

where

$$\alpha_k = \begin{cases} 1, & k = CH_4 \equiv \text{fuel}, \\ 2, & k = O_2 \equiv \text{ox}, \\ -1, & k = CO_2, \\ -2, & k = H_2O, \\ 0, & k = N_2, \end{cases}$$

as previously used by Mohamad et al. [20]. The pre-exponential factor is equal to $A = 1 \times 10^{10}$ [m^3/(kg s)] and the activation energy to $E = 1.4 \times 10^8$ [J/kmol]. The nitrogen mass fraction was calculated as the remaining part of the unit sum of all species.

For radiation purposes the porous material was considered as a diffuse gray body together with a non-radiating gas mixture. The heat source term $\partial Q_r/\partial x$ due to radiation, which appears in Eq. (4), is calculated from the radiative heat transfer equations [21]:

$$\mathbf{s}\cdot\nabla I = \beta\left((1-\omega)I_b - I + \frac{\omega}{4\pi}\int_{4\pi} I(\mathbf{s}_i)\Phi(\mathbf{s}_i,\mathbf{s})\,d\Omega_i\right),$$

$$\nabla\cdot Q_r = (1-\omega)\beta\left(4\pi I_b - \int_{4\pi} I(\mathbf{s})\,d\Omega\right). \tag{6}$$

Under the 1D assumption Eqs. (6) are simplified as

$$\mu\frac{dI}{d\tau} = (1-\omega)I_b - I + \frac{\omega}{2}\int_{-1}^{1} I(\tau,\mu_i)\Phi(\mu,\mu_i)\,d\mu_i, \tag{7}$$

$$\frac{dQ_r}{d\tau} = (1-\omega)\left(4\pi I_b - 2\pi\int_{-1}^{1} I(\tau,\mu)\,d\mu\right) \tag{8}$$

with boundary conditions given by

$$I(\tau=0) = \frac{\sigma}{\pi}T_0^4, \qquad I(\tau=\beta L) = \frac{\sigma}{\pi}T_L^4, \tag{9}$$

where $\tau = \beta x$ is the optical depth, and $I_b = \frac{\sigma}{\pi}T_s^4$.

The radiative heat transfer term in the solid equation was calculated, by default, using the discrete-ordinates method [21] (S_8 approximation) applied to Eqs. (7), (8), and (9). The Roseland diffusion approximation

$$\frac{dQ_r}{d\tau} = -\frac{d}{d\tau}\left(\frac{16\sigma}{3}T_s^3\frac{dT_s}{d\tau}\right) \tag{10}$$

is a simplified model for radiative heat transfer occurring in optically thick media (with high characteristic τ) and far away from the porous solid boundaries [15]. The linear stability analysis results provided with this simple model will be used for comparison with those obtained with the discrete-ordinates method.

2.2. Boundary conditions and interface treatments

Two computational domains were considered. In the first one, referred to as the GSG-domain, the gas-

Table 1
Solid domain (S) boundary conditions (CC′ and DD′)

Domain	Conservation	CC′ inlet	DD′ outlet
S	Mass	Eq. (11)	Eq. (12)
	Species	Eq. (13)	Eq. (14)
	Gas energy	Eq. (15)	$\phi\lambda_g \frac{\partial T_g}{\partial x} + (1-\phi)H_s(T_g - T_s) = 0$
	Solid energy	Eq. (17)	Eq. (18)

phase boundary conditions were extended upstream and downstream from the foam (see Fig. 1a) in order to ensure that the submerged and surface flames were not influenced by the inlet/outlet boundary conditions. The second configuration (see Fig. 1b), which will be referred as the S-domain, is also considered, where the inlet/outlet porous solid boundaries are coincident with the boundaries of the computational domain. Very often this last configuration is employed in the study of submerged flames. The boundary conditions that are common to both computational domains are the inlet Dirichlet conditions for mass, species, and gas energy, and the outlet Neumann conditions for mass and species; see the equations

Continuity equation b.c.

$$\text{inlet: } \rho_g u = \rho_g u|_{in}, \tag{11}$$

$$\text{outlet: } \frac{\partial(\rho_g u)}{\partial x} = 0. \tag{12}$$

Species transport equation b.c.

$$\text{inlet: } Y_k = Y_k|_{in}, \tag{13}$$

$$\text{outlet: } \frac{\partial Y_k}{\partial x} = 0. \tag{14}$$

Gas energy equation b.c.

$$\text{inlet: } T_g = T_g|_{in}, \tag{15}$$

$$\text{outlet: } \frac{\partial T_g}{\partial x} = 0. \tag{16}$$

The inlet/outlet boundary conditions for the solid energy equation, in the case of the S-domain, are obtained by an energy balance at the gas–solid interfaces, as presented in the equations

Solid energy equation b.c.

solid inlet:

$$-\lambda_s \frac{\partial T_s}{\partial x} - H_s(T_g - T_s) + \epsilon\sigma\left(T_s^4 - T_0^4\right) = 0, \tag{17}$$

solid outlet:

$$\lambda_s \frac{\partial T_s}{\partial x} - H_s(T_g - T_s) + \epsilon\sigma\left(T_s^4 - T_L^4\right) = 0, \tag{18}$$

where $H_s = H_v/a_s$, $T_0 = T_g|_{in}$, and $T_L = T_\infty$.

The boundary condition for the gas energy at the outlet is also obtained from an energy balance. Table 1 summarizes the S-domain boundary conditions used to close Eqs. (1)–(4).

The GSG-domain inlet/outlet boundary conditions are specified by Eqs. (11) to (16), for mass, species and gas energy, respectively. The outlet gas energy boundary condition, given by Eq. (16), corresponds to a Neumann condition.

The gas–solid interfaces CC′ and DD′ are located inside the GSG-domain and create a void fraction discontinuity that may contaminate the solution. The numerical treatment of these interfaces was investigated in detail to avoid misinterpretations of the linear stability analysis and to avoid any perturbation in the solution fields induced by erroneous numerical treatments of the interfaces. Table 2 summarizes the several interface treatments used in Eqs. (1)–(4). One possibility to treat the interface is to assume that there is a discontinuity; see [15]. The numerical treatment at CC′ and DD′ is listed in Table 2 and was named GSG1. A gas energy balance at the interfaces establishes the following conditions:

CC′ interface:

$$\lambda_g \frac{\partial T_g}{\partial x}|_- + (1-\phi)H_s(T_g - T_s) = \phi\lambda_g \frac{\partial T_g}{\partial x}|_+, \tag{19}$$

DD′ interface:

$$\phi\lambda_g \frac{\partial T_g}{\partial x}|_- + (1-\phi)H_s(T_g - T_s) = \lambda_g \frac{\partial T_g}{\partial x}|_+. \tag{20}$$

Another option is to eliminate the interface discontinuity, see [2], replacing it by a linear variation of the solid properties in the control volume interface vicinity, GSG3 conditions. Consequently, Eqs. (2) and (3) are used with the porosity varying linearly from $\phi = \phi_s$ inside the solid to $\phi = 1$ outside. The heat convection coefficient also varies linearly from H_v to zero, outside the solid. At CC′ it is assumed that radiation and convection are neglected in Eq. (17) because the gas and solid temperatures are similar.

In order to identify the influence of radiation losses at the hot solid outlet, another case was created (named GSG2). The only difference between cases GSG3 and GSG2 corresponds to the DD′ interface where, after neglecting radiation, Eq. (18) is simplified to

$$\lambda_s \frac{\partial T_s}{\partial x} - H_s(T_g - T_s) = 0. \tag{21}$$

Table 2
Gas–solid–gas domain (GSG) boundary conditions (AA′ and BB′) and interface treatments (CC′ and DD′)

Domain	Conservation	AA′	BB′	CC′	DD′
GSG1	Mass	Eq. (11)	Eq. (12)	–	–
	Species	Eq. (13)	Eq. (14)	$\frac{\partial Y_k}{\partial x}\vert_- = \phi \frac{\partial Y_k}{\partial x}\vert_+$	$\phi \frac{\partial Y_k}{\partial x}\vert_- = \frac{\partial Y_k}{\partial x}\vert_+$
	Gas energy	Eq. (15)	Eq. (16)	Eq. (19)	Eq. (20)
	Solid energy	–	–	Eq. (17)	Eq. (18)
GSG2	Mass	Eq. (11)	Eq. (12)	–	–
	Species	Eq. (13)	Eq. (14)	(*)	(*)
	Gas energy	Eq. (15)	Eq. (16)	(*)	(*)
	Solid energy	–	–	$\frac{\partial T_s}{\partial x} = 0$	Eq. (21)
GSG3	Mass	Eq. (11)	Eq. (12)	–	–
	Species	Eq. (13)	Eq. (14)	(*)	(*)
	Gas energy	Eq. (15)	Eq. (16)	(*)	(*)
	Solid energy	–	–	$\frac{\partial T_s}{\partial x} = 0$	Eq. (18)

Note. (*) linear variation of ϕ and H_V.

Table 3
Problem parameters and physical properties

ϕ_s	0.8	ρ_s	3.0×10^3 kg/m^3
ρ_g	0.3 kg/m^3	C_{ps}	0.35 kJ/(kg K)
C_{pg}	1.4 kJ/(kg K)	λ_s	0.8 W/(m K)
λ_g	0.1 W/(m K)	β	1500.0 m^{-1}
C_{pk}	1.4 kJ/(kg K)	ω	0.8
D_k	3.0×10^{-4} m^2/s	ϵ	0.85
H_v	2.0×10^6 W/(m^3 s)	T_∞	300 K
a_s	4000.0 m^{-1}	$T_g\vert_{in}$	300 K

2.3. Numerical model

The equations presented above were numerically solved using a modified version of the PREMIX code [22,23] that incorporates the solid energy balance equation (4) and the heat exchange between gas and solid phases.

The computational domain was subdivided according to the gas temperature spatial variation in an adaptive mesh refinement strategy, and for each of the subdomains a uniform mesh was used, with a smooth grid expansion or contraction transition between the domains. Grid independence of the solution was achieved with about 800 grid points in the 1D domain. One of the two following strategies was used to search for the solution: (i) imposing the flame location and calculating the flow velocity or (ii) imposing the inlet velocity and calculating the flame location. These two methods lead to virtually identical solutions, but in some cases the second methodology presents convergence problems; see also [15]. The numerical model constitutes a standard procedure for 1D premixed combustion in porous media, and it was previously validated with excellent agreement against experimental temperature and concentration data [23] and also against other predictions [15].

2.4. Linear stability analysis

The evolution of small disturbances in the system is given by the linearized form of Eqs. (1)–(4), obtained by the standard decomposition of the variables into a mean solution and a perturbation [24],

$$f(x,t) = \bar{f}(x) + f'(x,t), \tag{22}$$

where f represents T_g, T_s, Y_k, or u. The linear stability analysis is conducted assuming all physical and transport properties to be constant, as listed in Table 3. Therefore the variables of the problem were reduced to T_g, T_s, Y_k, and u. Equation (1) falls out of this analysis because, by assuming ρ_g constant, the perturbation u' in the flow velocity must be zero to satisfy continuity. This assumption suppresses hydrodynamic disturbances, leaving just the diffusion-thermal effects, and previous studies showed that realistic qualitative results are obtained [18,19].

Replacing Eq. (22) into the remaining Eqs. (2)–(4) and after linearization, the equations for species and gas and solid energy that model the evolution of small disturbances read as

$$\frac{\partial Y_k'}{\partial t} + u\frac{\partial Y_k'}{\partial x} - D_k\frac{\partial^2 Y_k'}{\partial x^2} - \dot{\omega}_k'\frac{\mathrm{MW}_k}{\rho} = 0, \tag{23}$$

$$\frac{\partial T'_g}{\partial t} + u\frac{\partial T'_g}{\partial x} - \frac{\lambda_g}{\rho C_{pg}}\frac{\partial^2 T'_g}{\partial x^2} - \sum_k \frac{C_{pk} D_k}{C_{pg}}\left(\frac{\partial Y'_k}{\partial x}\frac{\partial \bar{T}_g}{\partial x} + \frac{\partial \bar{Y}_k}{\partial x}\frac{\partial T'_g}{\partial x}\right) + \sum_k \dot{\omega}'_k \frac{h_k \mathrm{MW}_k}{\rho C_{pg}} + \frac{H_v}{\phi\rho C_{pg}}\left(T'_g - T'_s\right) = 0, \quad (24)$$

$$\frac{\partial T'_s}{\partial t} - \frac{\lambda_s}{\rho_s C_{ps}}\frac{\partial^2 T'_s}{\partial x^2} - \frac{H_v}{\rho_s C_{ps}}\left(T'_g - T'_s\right) + \frac{1}{\rho_s C_{ps}}\frac{\partial Q'_r}{\partial x} = 0, \quad (25)$$

where the reaction rate perturbation $\dot{\omega}'_k$ is given by

$$\dot{\omega}'_k = -\alpha_k \frac{\rho_g^2}{\mathrm{MW}_{fuel}} A\left(\bar{Y}_{fuel}\bar{Y}_{ox}\frac{E}{R\bar{T}_g^2}T'_g + Y'_{fuel}\bar{Y}_{ox} + \bar{Y}_{fuel}Y'_{ox}\right)e^{-E/(R\bar{T}_g)}. \quad (26)$$

The boundary conditions for Eqs. (23)–(25) can be obtained with the same assumptions listed in Tables 1 and 2 but replacing each problem variable f by its perturbation f' (where $u'|_{in} = Y'_k|_{in} = T'_g|_{in} = 0$). The only exceptions are related to the last term of Eqs. (17) and (18), which become, after linearization, equal to $4\epsilon\sigma\bar{T}_s^3 T'_s$.

It is not possible to include radiative heat transfer perturbation equations in the linear stability analysis because an unsteady equation system for radiation does not exist. Therefore, in Eq. (25), the radiative flux rate perturbation $\partial Q'_r/\partial x$ must be given as an explicit function of T'_s.

The radiative flux rate perturbation corresponding to the Roseland approximation, see Eq. (10), is given by

$$\frac{\partial Q'_r}{\partial x} = -\frac{16\sigma\bar{T}_s^2}{3\beta}\left(\bar{T}_s\frac{\partial^2 T'_s}{\partial x^2} + \frac{\partial^2 \bar{T}_s}{\partial x^2}T'_s\right). \quad (27)$$

An equation for $\partial Q'_r/\partial x$ is not so straightforward when the discrete-ordinates method is used to solve the 1D radiative heat transfer Eqs. (7)–(9), therefore the following procedure is proposed. First, Eqs. (7), (8), and (9) were linearized. Second, by applying the S_2 approximation to the resulting linear equations, an ODE system was obtained, and its analytical solution was calculated using the software MATHEMATICA [25], yielding the radiative flux rate perturbation given by

$$\frac{\partial Q'_r}{\partial x} = (1-\omega)\beta\left(16\sigma\bar{T}_s^3 T'_s\right) - (1-\omega)\beta\left(2\pi\alpha(x)\left[\int_0^x a(t,x)\bar{T}_s^3(t)T'_s(t)\,dt + \int_x^1 b(t,x)\bar{T}_s^3(t)T'_s(t)\,dt\right]\right), \quad (28)$$

where

$$\alpha(x) = -\frac{6e^{-6\sqrt{5}x}}{5 - 3\sqrt{5} + (5+3\sqrt{5})e^{12\sqrt{5}}}, \quad (29)$$

$$a(t,x) = \frac{1701}{250{,}000}\left[(1+\sqrt{5})e^{12\sqrt{5}} - (\sqrt{5}-1)e^{12\sqrt{5}x}\right] \times \left[\cosh(6\sqrt{5}t) + \sqrt{5}\sinh(6\sqrt{5}t)\right], \quad (30)$$

$$b(t,x) = \frac{1701}{125{,}000}e^{6\sqrt{5}(1+x)} \times \left[6\sqrt{5}\cosh\left(6\sqrt{5}(1-t+x)\right) - 2\cosh\left(6\sqrt{5}(-1+t+x)\right) + \sqrt{5}\sinh\left(6\sqrt{5}(1-t+x)\right)\right] \quad (31)$$

with $\beta = 1500.0\ \mathrm{m}^{-1}$ and $\omega = 0.8$. Since the problem is one-dimensional, with homogeneous porous media, the steady solutions calculated with S_8 or S_2 approximation were found to be very similar. Therefore, the S_2 was preferred for the linear stability analysis, because it simplifies the treatment of Eq. (28) with negligible accuracy loss.

The integrals in Eq. (28) were discretized by the trapezoidal rule to assign the source term in Eq. (25).

The set of Eqs. (23)–(25) accepts a nontrivial solution in the form, see, e.g., [24],

$$Y'_k(x,t) = \delta_k(x)e^{\theta_k t}, \quad T'_g(x,t) = \tau_g(x)e^{\theta_g t}, \quad T'_s(x,t) = \tau_s(x)e^{\theta_s t}, \quad (32)$$

where the complex numbers θ_j ($j = k, g, s$) are the system eigenvalues. The system is said to be stable if the real part of the system eigenvalues is negative ($\mathrm{Re}(\theta) < 0$) for all θ_j; otherwise the small perturbations (32) will be amplified and the solution will be unstable. The real part of the system eigenvalues can be ordered as $\mathrm{Re}(\theta_1) > \mathrm{Re}(\theta_2) > \cdots$, where the highest value is the critical one ($\mathrm{Re}(\theta_1) = \mathrm{Re}(\theta_{cr})$) for the system stability condition.

After discretizing Eqs. (23)–(25) together with Eqs. (32) with the same scheme used to compute the steady solution, a matrix eigenvalue problem was obtained (with dimension around 4800×4800). This matrix was solved to find the system eigenvalues that determine the stability condition of each steady solution.

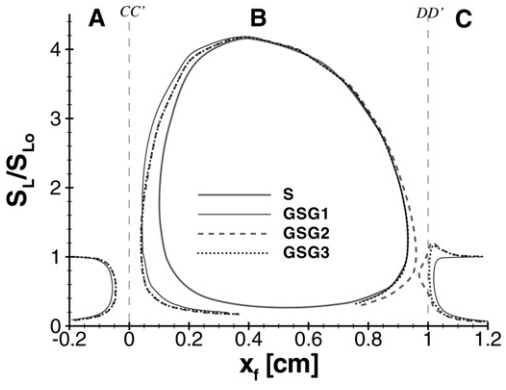

(a)

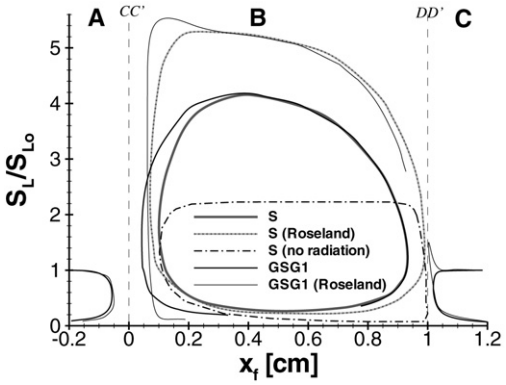

(b)

Fig. 2. Stabilization diagram with surface and submerged steady flames stabilized using (a) several b.c. sets; (b) various radiation models.

3. Results

3.1. Results of steady solutions

Numerical solutions were obtained for two computational domains (GSG-domain and S-domain); see Figs. 1a and 1b, respectively. Several interface conditions, listed in Table 2, were used in the GSG-domain and are referred to as GSG1, GSG2, and GSG3. In addition, two radiation models were employed (the discrete-ordinates method (S_8) used by default and the Roseland approximation), and the case with absence of radiative heat transfer was also considered. Extensive comparison with available experimental data or calculations was conducted to validate the numerical model [10,23], and numerical predictions reported by [15] were virtually reproduced, as examples of the validation process.

The calculated steady solutions are presented in the stabilization diagrams of Figs. 2a and 2b, obtained with the different interface treatments and different radiation models, respectively. The flame position (x_f) was assumed to be located where the maximum heat release rate occurs (where $\partial T_g/\partial x$ is maximum) [2]. It is observed that the flame can be stabilized in three distinct combustion zones, in agreement with [11]: zone (B) corresponds to submerged flames inside the porous foam, and zones (A) and (C) to surface flames upstream or downstream of the solid, respectively. Submerged flames can have flame speeds greater than free flame speeds ($S_L > S_{Lo}$), and they show two distinct x_f for the same S_L value, corresponding to the upstream and downstream solutions. Similarly, both submerged and surface flames exhibit two S_L values for one given x_f, corresponding to the upper and lower solutions [12,13].

The gas and solid temperatures, as well as the species concentration evolution corresponding to upper and lower solutions existing in zones A, B, and C, are presented in Fig. 3. The upstream surface flames (zone A) are showed in Figs. 3a and 3b, the submerged flame (zone B) in Figs. 3c and 3d, and the downstream surface flames (zone C) in Figs. 3e and 3f. It can be seen that these flames are influenced in different ways depending on their position relative to the porous solid, mainly due to the levels of heat recirculation and heat loss. Each pair of upper/lower solutions present the same x_f, but their temperature profiles are clearly different. For instance, the upper solutions present higher combustion temperature and S_L values than the lower solutions. This is due to the higher heat release rate in the upper flame solutions which also creates a steeper temperature gradient in the upper flame front. It can also be noted that upper solutions of submerged flames (zone B) present gas temperatures in a clear nonequilibrium with the solid, contrary to the lower solutions.

Figs. 3b, 3d, and 3f show that the reaction zone, where the species molar fraction changes, is thicker for the lower flames and the species production rates are smaller, promoting incomplete reactions in zones A and B, see Figs. 3b and 3d, respectively, but not in zone C, see Fig. 3f. This can be explained by the position of the porous solid relative to the flame front, which will also have deep implications for the linear stability analysis. The porous solid acts like a heat sink on the upstream surface flames (zone A), dissipating energy out of the flame front and decreasing the products temperature, affecting mainly the lower solutions, which have weaker reaction rates. The heat recirculation created by the solid in the submerged flames (zone B) also decreases the products temperature but improves the combustion reaction, and in general the reactions of the lower solutions in zone B are less incomplete than the reactions of the lower solutions in zone A; see Figs. 3b and 3a, respectively. In the downstream surface flames (zone C), the solid recirculates heat from the flame front, preheating the reactants without decreasing the products

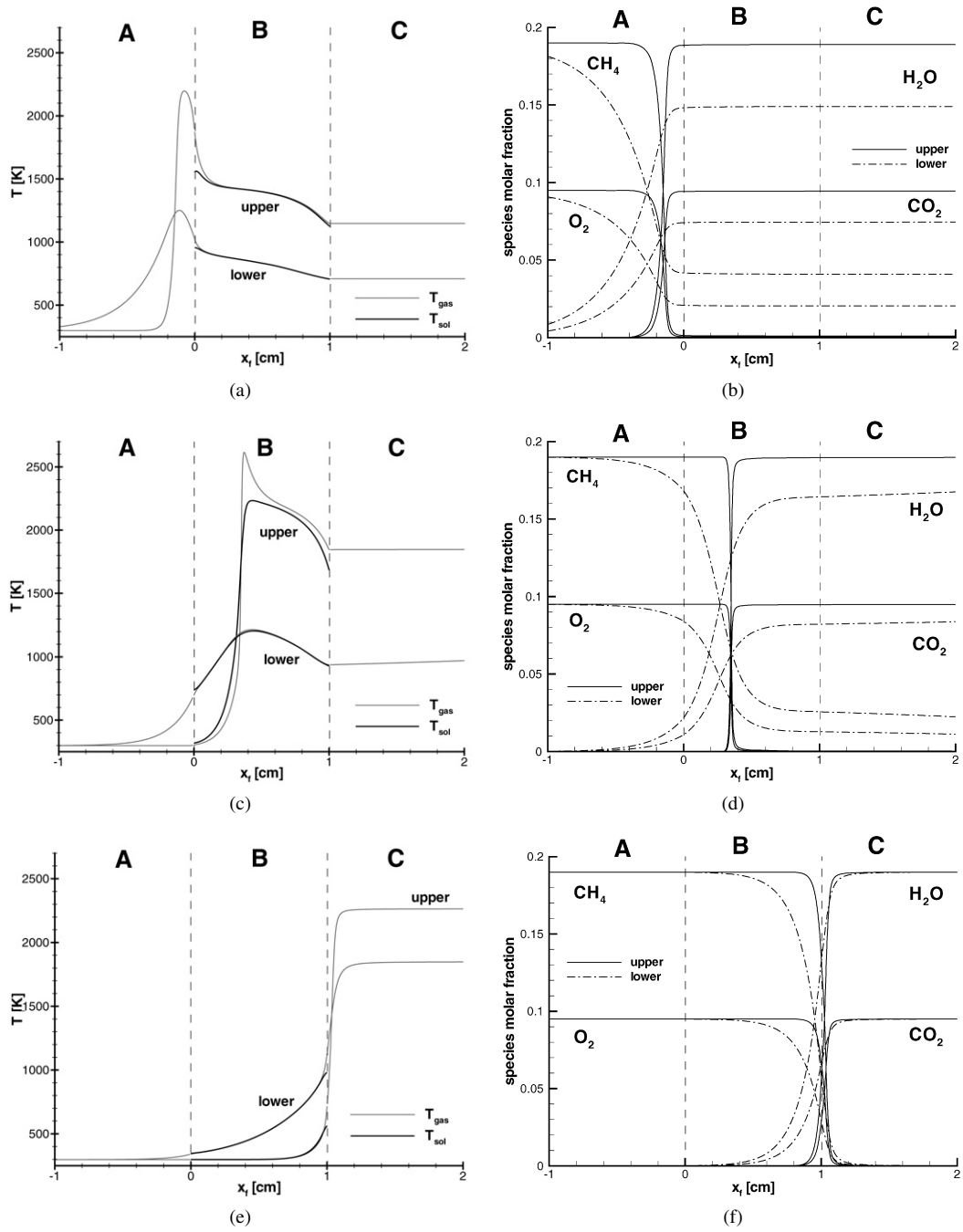

Fig. 3. Gas and solid temperature as well as gaseous mixture species (excluding N_2) profiles of upper/lower flame pairs obtained with GSG1 treatment: (a), (b) zone A surface flames ($x_f = -0.13$ cm); (c), (d) zone B submerged flames ($x_f = 0.34$ cm); (e), (f) zone C surface flames ($x_f = 1.05$ cm).

temperature, and, although the heat recirculation is less effective than in the submerged flames, the lower solutions present complete reactions.

The several interface treatments and radiation models applied to the solid energy equation (4) do not directly affect the chemical reactions in the gas phase, but only through the modification of the solid temperature distribution leading to different flame behaviors. Inspection of Fig. 2a for submerged flames, zone B, shows that the results obtained in the GSG-domain, ir-

respective of the interface treatments (GSG1, GSG2, and GSG3 interface conditions), or in the S-domain display very similar (x_f, S_L) curves. Far away from the gas–solid interfaces, the model solutions obtained with different interface treatments almost match, and near the interface regions small differences occur. Close to the CC′ interface, the S-domain flames are located at a relatives large distance from CC′ because a Dirichlet b.c. ($T_g = 298$ K) is imposed here. The GSG2 and GSG3 flames are stabilized with a smaller S_L than GSG1 flames for the same position, because the solid does not preheat the reactants at the CC′ interface and the combustion temperature is lower. Although the solid does not lose heat by radiation from the CC′ interface to the upstream environment, this is not important due to the low solid temperature at the interface (∼600 K). In the case of GSG2 flames, the solid does not lose heat by radiation from the DD′ interface to the downstream environment and this phenomenon cannot be neglected here because of the high solid temperature at the interface (∼1700 K); therefore these flames tend to stabilize closer to DD′ than the other flames (S, GSG1, GSG3) to compensate for the smaller heat loss.

In zones A and C, far away from the gas/solid interfaces CC′ and DD′, all model solutions (GSG1, GSG2, GSG3) tend to overlap as the flames are becoming free flames and $S_L = S_{Lo}$ (not changing with x_f). The CC′ interface treatment has small influence on the upstream surface flames (zone A). The adiabatic CC′ treatment imposed on the solid temperature, for GSG2 and GSG3 solutions, implies that less heat is removed from the upstream surface flames and consequently they can be stabilized closer to CC′ interface.

Near the DD′ interface, some differences can be seen among the GSG-domain solutions. The flames obtained with GSG2 and GSG3 can be stabilized closer to DD′. For GSG2 solutions, the solid does not lose heat by radiation to the environment; therefore the flames are not able to dissipate a sufficient amount of heat and tend to stabilize deeper inside region B, where the porous solid will compensate by recirculating more heat to the reactants [16]. Although it is stated referred by [15] that the surface flames present $S_L < S_{Lo}$, it is observed that the GSG2 and GSG3 solutions can display regions with $S_L > S_{Lo}$. This is due to the DD′ interface treatment in the species and gas equations (2) and (3). After rearranging the convection and diffusion terms of Eq. (3) the following result is obtained:

$$\phi\rho_g u C_{pg}\frac{\partial T_g}{\partial x} - \frac{\partial}{\partial x}\left(\phi\lambda_g\frac{\partial T_g}{\partial x}\right) = \left(\phi\rho_g u - \frac{\partial\phi}{\partial x}\frac{\lambda_g}{C_{pg}}\right)C_{pg}\frac{\partial T_g}{\partial x} - \phi\lambda_g\frac{\partial^2 T_g}{\partial x^2}. \quad (33)$$

In the first term, on the right side of Eq. (33), appears a term that represents the effective mass flux on the interface (where $\partial\phi/\partial x \neq 0$), which is smaller than the real mass flux ($\phi\rho_g u$). Therefore the solution tends to increase S_L to compensate for this deficit, explaining the region with $S_L > S_{Lo}$ near the DD′ interface. If the transition condition for ϕ is made smoother, by decreasing $\partial\phi/\partial x$, zones with $S_L > S_{Lo}$ will no longer exist.

Fig. 2b shows the effect of the discrete-ordinates and Roseland radiation models as well as the absence of solid radiation on the flame solutions in the stabilization diagram. The Roseland radiation model drastically increases the upper flames S_L values compared with the results obtained using the discrete-ordinates radiation model, while for the lower flames the S_L values slightly decrease. These differences are due to the optically thick assumption, which reduces the heat diffusion through the solid and improves the heat recirculation in the flame front region. The bigger differences in the upper solutions result from the higher solid temperature, which amplifies the influence of the radiation term in the solid energy equation. Near the solid boundaries there are also notorious differences, but the optically thick assumption embodied in the Roseland model is not valid [15] in this region, while the discrete-ordinates model is a realistic one. For the surface flames there are several subzones in A and C where the Roseland model produces results similar to the discrete-ordinates model, because the flame front region is outside the porous solid and radiation loses importance due to the lower solid temperature.

Fig. 2b also shows that for the S-domain case, the solutions without radiation heat transfer induce erroneous solutions, showing notorious differences from the solutions obtained with the inclusion of radiation. The maximum S_L value is approximately half the value obtained with radiation, and deep inside the solid S_L assumes a constant value. This is because the heat recirculation created by the porous solid is poorly made only by conduction, which acts on a very short length scale compared with the radiation phenomena. The previous discussion emphasizes that solid radiation is an important feature in porous media combustion and cannot be ignored; therefore its mechanism may also be determinant for a linear stability analysis.

3.2. Results of linear stability analysis

After comparing the effect of the several interface treatments and radiation models on the flame stabilization mechanism, a discussion of the linear stability of these flames is presented in this section. The stabilization diagrams of the S-domain solutions, with

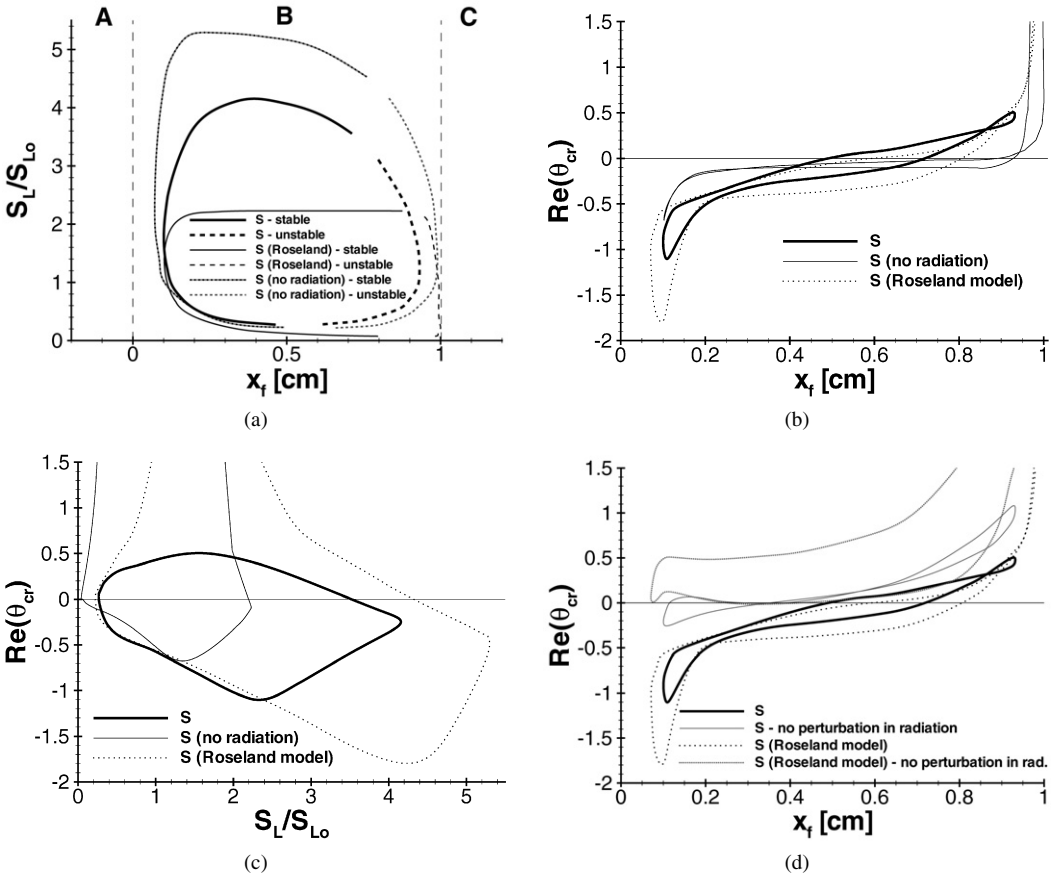

Fig. 4. S-domain submerged flames obtained using the several radiation models and including the stability character of the solutions: (a) stabilization diagram; (b) real part of the critical eigenvalue vs flame position; (c) real part of the critical eigenvalue vs relative flame speed; (d) influence of the radiation perturbation on the real part of the critical eigenvalue.

the discrete-ordinates or Roseland models for radiation and without radiation, are presented in Fig. 4a. The stabilization diagrams of the GSG-domain solutions are shown in Figs. 5a, 5b, and 5c for clarity of comparison among the GSG1, GSG2, and GSG3 solutions, respectively. The stable and unstable flame regions are made distinct by continuous or dashedlines, respectively. The real part of the critical eigenvalue $\mathrm{Re}(\theta_{\mathrm{cr}})$ corresponding to each flame is shown in order to quantify the degree of stability obtained; see Figs. 4b, 4c, 4d, and 6.

Fig. 4a shows the stabilization diagram for the submerged flames (zone B) in the S-domain. The linear stability analysis displays unstable flames in the downstream region of the solid, for both lower and upper solutions. It has been suggested by [11] that, for a flame to be stable, its downstream displacement must be compensated for by an increase in the flame speed ($\partial(S_{\mathrm{L}}/S_{\mathrm{Lo}})/\partial x_{\mathrm{f}} > 0$), creating a tendency in the flame to return back to its original position. The present results show that this stability condition was only found for upper flames without radiation. Fig. 4a shows upper stable flames with $\partial(S_{\mathrm{L}}/S_{\mathrm{Lo}})/\partial x_{\mathrm{f}} < 0$ in the middle region of the porous media, suggesting that solid radiation increases the stability of upper submerged flames, shifting the stable–unstable transition to regions where $\partial(S_{\mathrm{L}}/S_{\mathrm{Lo}})/\partial x_{\mathrm{f}}$ is negative. Fig. 4a also shows that for the solutions obtained with radiation (discrete-ordinates or Roseland models), the stable–unstable transition zone is located earlier in the downstream direction than for the solutions where no radiation is considered. This can be explained by the radiative heat losses from the DD′ interface to the downstream environment, which do not exist in the absence of solid radiation. The above discussion suggests that the effect of solid radiation on the flame stability of submerged flames is dictated by two phenomena acting in opposite ways: the heat recirculation, which increases the submerged flame stability, and the radiative heat loss to the downstream environment, which decreases the stability of submerged flames located close to the DD′ interface.

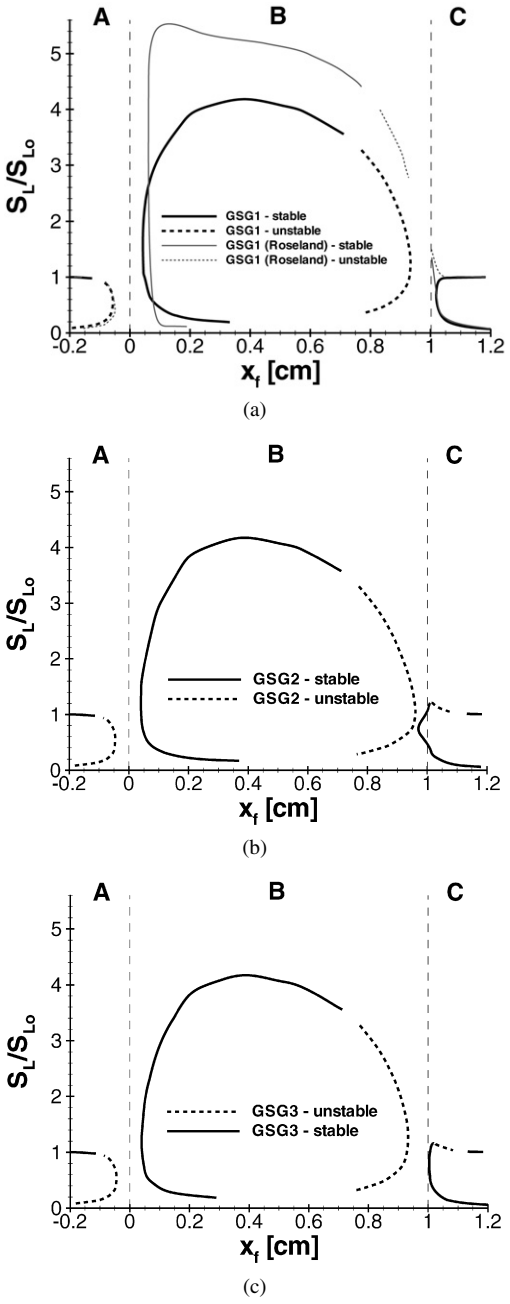

Fig. 5. GSG-domain stabilization diagrams with the stability character of the solutions: (a) GSG1 solutions obtained with the several radiation models; (b) GSG2 solutions; (c) GSG3 solutions.

Figs. 4b and 4c show the values of $\mathrm{Re}(\theta_{\mathrm{cr}})$ as a function of flame position x_{f} and relative flame speed $S_{\mathrm{L}}/S_{\mathrm{Lo}}$, respectively. It is possible to conclude that the upstream flames are the most stable ones, and the flames in the middle of the porous foam are least stable, up to become unstable in the downstream region. This is in agreement with what experimental evidence suggests, stable submerged flames were found by [12] only in the upstream region of the porous burner; in [13], lower submerged flames were stabilized in the downstream region by applying external heating, and those were observed to oscillate. Fig. 4b shows that the submerged flames calculated without radiation are more stable in the upstream part of the solid, where $\partial(S_{\mathrm{L}}/S_{\mathrm{Lo}})/\partial x_{\mathrm{f}}$ is higher, suggesting that this variable is a determining factor in the flame stability, in agreement with [11]. It can also be noted in Figs. 4b and 4c that the upper flames are more stable than the lower flames, maybe because lower flames present a much lower temperature and the stabilizing effect of radiation is less effective; see Fig. 3d. Observing the influence of the solid radiation on $\mathrm{Re}(\theta_{\mathrm{cr}})$, one can conclude that it increases the flame stability.

For a better understanding of how the solid radiation can contribute to the flame stability, linear stability analysis was also performed, neglecting the radiative flux rate disturbance $\partial Q'_{\mathrm{r}}/\partial x$ in Eq. (25). Fig. 4d shows the effect of the radiation perturbation on the value of $\mathrm{Re}(\theta_{\mathrm{cr}})$ for the S-domain solutions calculated with the discrete-ordinates model or with the Roseland approximation. It can be seen that, in both cases, the value of $\mathrm{Re}(\theta_{\mathrm{cr}})$ is shifted in the negative direction if the radiative flux rate disturbance is excluded from the linear stability analysis. It can be concluded that the flame stability decreases in the absence of radiation perturbation, suggesting that the radiation acts like a damper that dissipates the solid temperature disturbances T'_{s}.

Fig. 5 shows the stable and unstable solutions obtained for the GSG-domain with GSG1, GSG2, and GSG3 interface conditions. In respect to the submerged flames (zone B), the stability analysis provides identical conclusions for the GSG- and S-domain with radiative heat transfer. The transition zone from stable to unstable steady solutions is independent of the interface treatments considered (S, GSG1, GSG2, GSG3), because it occurs far from the interfaces; see Fig. 6a. Since the radiative heat losses to the downstream environment have been neglected in the GSG2 interface treatment, the resulting submerged flames existing in the downstream region are less unstable than the ones calculated with the other interface treatments (GSG1, GSG3). Also, the upstream submerged flames calculated with GSG2 and GSG3 treatments, which assume an adiabatic condition for the solid at the CC′ interface, are less stable than the solutions calculated with the GSG1 treatment, because the reactants are not preheated at the CC′ interface, leading to lower S_{L} values; see the respective eigenvalues in Figs. 6a and 6b.

For the upstream surface flames (zone A), the transition between stable and unstable flames is not

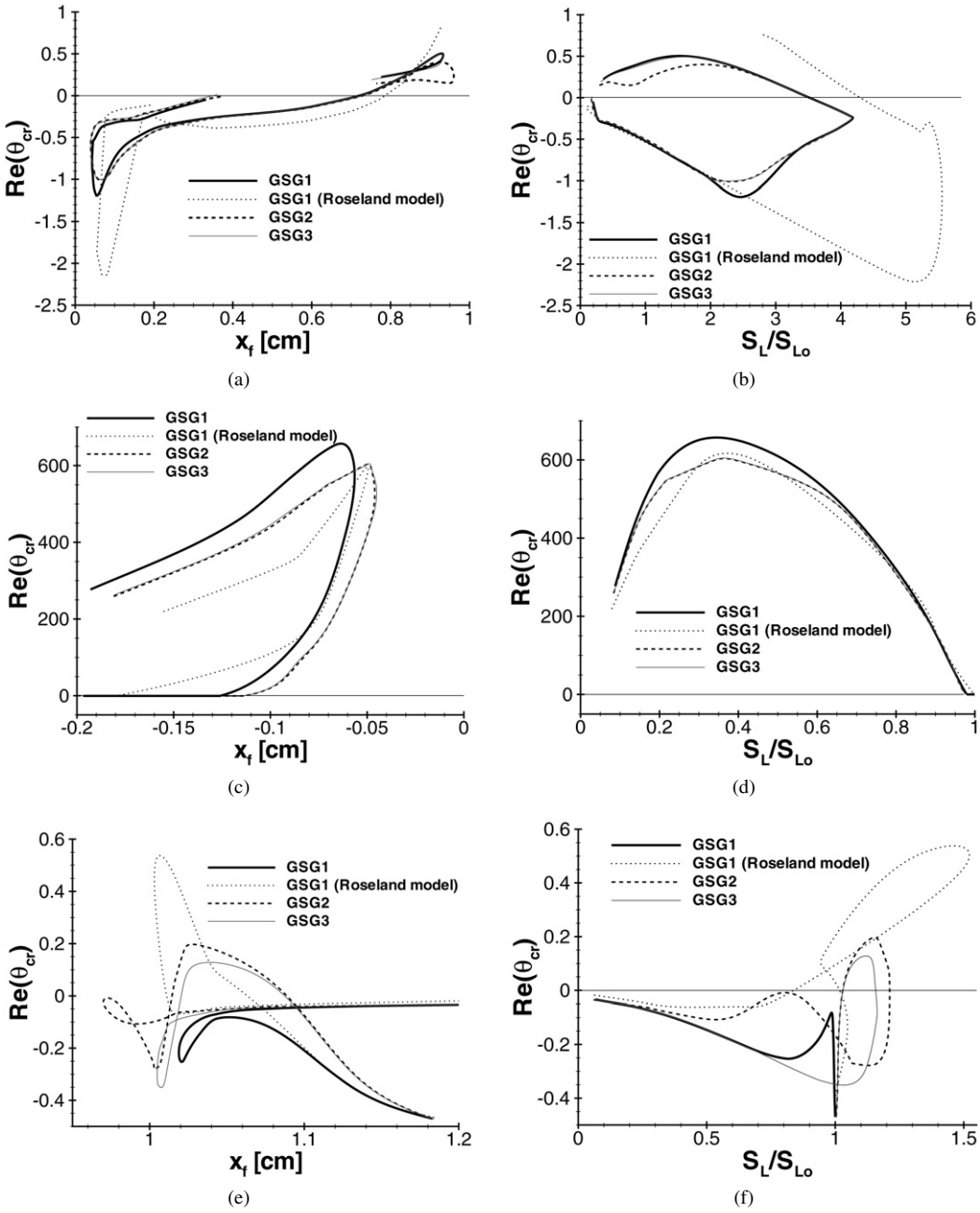

Fig. 6. GSG-domain submerged (zone B) and surface (zones A and C) flames stability: (a) real part of the critical eigenvalue vs flame position for zone B; (b) real part of the critical eigenvalue vs relative flame speed for zone B; (c) real part of the critical eigenvalue vs flame position for zone A; (d) real part of the critical eigenvalue vs relative flame speed for zone A; (e) real part of the critical eigenvalue vs flame position for zone C; (f) real part of the critical eigenvalue vs relative flame speed for zone C.

dependent on the interface treatment used, nor on the radiation model used. The upper solutions become unstable when $\partial(S_L/S_{Lo})/\partial x_f < 0$, in agreement with [11]; see Fig. 5. The stable upper flames can be considered free flames because the flame speed is constant and equal to S_{Lo}. Truly stable upstream surface flames do not exist in zone A because, as soon as the flame feels the solid, it becomes unstable, since the solid dissipates the heat from the flame front region. Kotani et al. [14] found stable flames ahead of a porous solid, but they used ceramic filters placed upstream and downstream of the porous solid

to reduce the radiative heat losses, and the upstream filter also provided heat recirculation to the reactants. Therefore the flames found in their experiments are different from the unstable upstream surface flames found in this study, mainly because the heat losses in their upstream flames were reduced, allowing more stable combustion. In our steady simulations it was observed that all the unstable upstream surface flames present an incomplete reaction, and the opposite was found for the stable "free" flames. Fig. 3b shows a stable upper flame (close to the limit of stability) and an unstable lower flame at the same location x_f.

Similarly to what happen in zone A, the upper solutions of downstream surface flames (zone C) also become unstable when $\partial(S_L/S_{Lo})/\partial x_f < 0$, but in this case the stability also depends on the radiation model used; see Fig. 5a. The upper solutions obtained with the Roseland radiation model show notorious differences from the solutions calculated with the discrete-ordinates model. The GSG2 and GSG3 upper solutions in zone C are unstable in regions where $\partial(S_L/S_{Lo})/\partial x_f < 0$ because radiation is not relevant in the gas domain and the stability is just dictated by the variation of S_L with x_f. The conclusion is similar for the submerged flames (zone B) when radiation was not incorporated in the model. For both upstream and downstream surface flames (zones A and C), the lower solutions are stable although $\partial(S_L/S_{Lo})/\partial x_f < 0$, and the argument given by [11] is applicable only to upper surface flames or submerged flames without radiation.

Figs. 6c and 6e show the real part of the critical eigenvalue $\mathrm{Re}(\theta_{cr})$ obtained from the linear stability analysis, as a function of x_f, for the upstream (zone A) and downstream (zone C) surface flames, respectively. The same information is shown in Figs. 6d and 6f, but $\mathrm{Re}(\theta_{cr})$ is given as a function of S_L/S_{Lo}. Since zone A displays very similar stable and unstable solutions for all the GSG treatments, the corresponding critical eigenvalues are also similar; see Figs. 6c and 6d. Relative to zone C, Fig. 6e shows that the stability of the upper flames decreases with the proximity of the flames to the solid, increasing again and showing a local maximum near the solid interface where the $\partial(S_L/S_{Lo})/\partial x_f$ value is higher. The GSG2 treatment neglects the radiation losses in the solid interface DD′ and consequently the flames tend to penetrate in the solid (zone B), creating a region with smaller $|\partial(S_L/S_{Lo})/\partial x_f|$ values where the flames are less stable than the GSG1 and GSG3 flames that remain in zone C. This can be related with [16], where it is observed that downstream surface flames existing in a hot environment tend to stabilize deep inside the solid, and a flashback window will be created if the environment temperature increases too much. For GSG2 and GSG3 the porosity is assumed to vary linearly in the interface vicinity and consequently in zone C there are upper flames with $S_L/S_{Lo} > 1$ that induce an unstable region, since outside the solid radiation is not relevant for the flame stability and $\partial(S_L/S_{Lo})/\partial x_f < 0$, respecting the argument proposed by [11].

4. Conclusions

Different features of inert porous media premixed CH_4/air combustion modeling have been investigated. The effect of different solid radiation models and gas/solid interface conditions on the stabilization of steady flames was studied by means of 1D numerical calculations. Special attention was given to the stability of these solutions and a linear stability analysis was performed with the influence of linearized solid radiation models.

(i) Different interface conditions can produce relatively similar solutions but some important differences can occur near the gas/solid interfaces, especially in the downstream surface flame zone. The use of a computational domain that includes only the finite porous solid may produce accurate results for submerged flames, but special attention is needed to the imposed inlet gas temperature (Dirichlet condition) because it influences the location of the upstream submerged flames near the inlet.

(ii) Inclusion of radiation is essential to obtain realistic results inside porous media. Calculations using the Roseland approximation can simulate the general effect of the solid radiation, but the error in predicting the flame speed can be enormous. Outside the solid, the radiation has a negligible effect except on the downstream surface flames near the gas/solid interface.

(iii) The influence of radiative heat transfer on the linear stability analysis was shown to be a very useful tool in the study of porous media premixed flame stability phenomena. Besides the information provided by the stabilization diagrams, it makes it possible to quantify the degree of stability for each flame. Moreover, the linearized Roseland radiation model and the accurate linearized S_2 approximation were implemented in linearized conservation equations, and they produce similar results on the stability analysis. By comparing linear stability analysis solutions, including and excluding radiation, it was possible to demonstrate the benefits of solid radiation in increasing the flame stability.

(iv) Several interface treatments were assessed on the flame stability analysis and shown to have a non-

negligible influence on the submerged and surface flames near the downstream gas/solid interface. The numerical treatment of the downstream gas/solid interface, GSG2 and GSG3, may induce regions where the downstream surface upper flames are unstable ($\partial(S_L/S_{Lo})/\partial x_f < 0$), but no unstable downstream surface flames were predicted with GSG1.

(v) Stability of the upper solutions for upstream and downstream surface flames was dictated by the signal of $\partial(S_L/S_{Lo})/\partial x_f$, in agreement with [11]. The same was found to be true for the upper solutions of the submerged flames calculated without radiation. However, the same was not observed for the stable upper submerged flames calculated with solid radiation. For this case, due to radiation, which increases flame stability, there are stable flames in regions where $(\partial(S_L/S_{Lo})/\partial x_f < 0)$. All the unstable upper flames present $\partial(S_L/S_{Lo})/\partial x_f < 0$, respecting the argument of [11]. For all the lower solutions (submerged and surface flames), the flame stability was also dictated by the signal of $\partial(S_L/S_{Lo})/\partial x_f$ because radiation is less relevant.

(vi) Linear stability analysis showed that submerged flames located on the downstream region of the porous solid are unstable, in agreement with the experiments [12,13]. Moreover, all upstream surface flames were found to be unstable and the experimental results of [14] do not contradict this observation and suggest that the radiation losses are an important phenomenon for the stability of upstream surface flames.

Acknowledgments

The support from EU under project FlameSOFC is gratefully acknowledged. M.A.A. Mendes and J.M.C. Pereira acknowledge the fellowships received from Fundação para a Ciência e a Tecnologia—FCT.

References

[1] D. Trimis, K. Wawrzinek, J. Comput. Appl. Mech. 5 (2) (2004) 367–381.
[2] A.J. Barra, J.L. Ellzey, Combust. Flame 137 (2004) 230–241.
[3] S. Mößbauer, O. Pickenäcker, K. Pickenäcker, D. Trimis, in: Fifth International Conference on Technologies and Combustion for a Clean Environment, Lisbon, 1999, pp. 519–523.
[4] F.J. Weinberg, Nature 233 (1971) 239–241.
[5] J.R. Howell, M.J. Hall, J.L. Ellzey, Prog. Energy Combust. Sci. 22 (1996) 121–145.
[6] A.A.M. Oliveira, N. Kaviany, Prog. Energy Combust. Sci. 27 (2001) 523–545.
[7] K. Hanamura, R. Echigo, Warme-Stoffubertragung 26 (1991) 377–383.
[8] S.B. Sathe, T.W. Tong, J. Heat Transfer 113 (1991) 423–428.
[9] Y. Yoshizawa, K. Sasaki, R. Echigo, Int. J. Heat Mass Transfer 31 (1988) 311–319.
[10] I. Malico, J.C.F. Pereira, ASME J. Heat Transfer 123 (2001) 951–957.
[11] J. Buckmaster, T. Takeno, Combust. Sci. Technol. 25 (1981) 153–158.
[12] D.K. Min, H.D. Shin, Int. J. Heat Mass Transfer 34 (1991) 341–356.
[13] Y.I. Lee, H.D. Shin, S.W. Baek, Combust. Sci. Technol. 112 (1996) 75–93.
[14] Y. Kotani, H.F. Behbahani, T. Takeno, in: Twentieth International Symposium on Combustion, 1984, pp. 2025–2033.
[15] D.J. Diamantis, E. Mastorakos, D.A. Goussis, Combust. Theory Modell. 6 (2002) 383–411.
[16] F.A. Lammers, L.P.H. de Goey, Combust. Flame 133 (2003) 47–61.
[17] J. Yuan, Y. Ju, C.K. Law, Combust. Flame 144 (2006) 386–397.
[18] V.N. Kurdyumov, M. Matalon, Combust. Flame (2007), doi:10.1016/j.combustflame.2007.07.003.
[19] B.H. Chao, Combust. Flame 126 (2001) 1476–1488.
[20] A.A. Mohamad, S. Ramadhyani, R. Viskanta, Int. J. Heat Mass Transfer 37 (1994) 1181–1191.
[21] M.F. Modest, Radiative Heat Transfer, McGraw–Hill, New York, 1993.
[22] R.J. Kee, J.F. Grcar, M.D. Smooke, J.A. Miller, A Fortran program for modeling steady laminar one-dimensional premixed flames, Report SAND85-8240, Sandia National Laboratories, 1996.
[23] Y.Y. Zhou, J.C.P. Pereira, Fire Mater. 22 (1998) 187–197.
[24] R. Vance, M. Micklavcic, I.S. Wichman, Combust. Theory Modell. 5 (2001) 147–161.
[25] Wolfram Research Inc., Mathematica—Version 5.2, Wolfram Research Inc., Champaign, IL, 2005.